DOI: 10.1002/ejic.201100205

Synthesis and Characterization of Single-Crystalline $MnFe_2O_4$ Ferrite Nanocrystals and Their Possible Application in Water Treatment

YingQi Wang,[a] RongMin Cheng,[b] Zi Wen,[a] and LiJun Zhao*[a]

Keywords: Manganese / Nanostructures / Magnetic properties / Water treatment

Manganese ferrite ($MnFe_2O_4$) nanospheres and nano-octahedra with a narrow size distribution were synthesized by a simple solvothermal method. Here, potassium permanganate ($KMnO_4$) was used as reactant and oxidant for the synthesis of $MnFe_2O_4$ ferrite nanocrystals. With the use of hydrazine hydrate, the oxidation rate of ferrous ions was kept under control, and the particle size of $MnFe_2O_4$ was limited. The results of control experiments reveal that alkalinity and type of solvent are important factors affecting the morphology and crystallization of $MnFe_2O_4$ nanocrystals. Both of the as-prepared samples exhibit ferromagnetic behavior at room temperature. Especially, the saturation magnetization of $MnFe_2O_4$ nanospheres with 50 nm diameter is 79 emu/g, which is among the best values reported so far. The nanoparticles also showed good performance in removal of pollutants like Congo red, Cr^{VI}, and Pb^{II} from water by adsorption, even at neutral pH.

Introduction

Magnetic nanoparticles with controlled size and shape are of great interest for both fundamental science and technological applications, because of their chemical and physical properties, and especially their magnetic properties. Among magnetic nanoparticles, manganese ferrites is a group of soft spinel ferrite materials with high magnetic permeability, high electrical resistance, and low loss, and they are widely used in many areas such as high-density magnetic recording,[1] ferrofluid technology,[2] electronic devices, magnetic resonance imaging (MRI),[3] microwave adsorption,[4] biomedical drug delivery,[5] and water treatment.[6,7] Nanosized spinel ferrite materials have been reported to give an excellent performance as catalyst or catalytic support for many chemical reactions, such as organic dehydrogenation,[8] catalytic oxidation, Fenton reaction,[9] and have found application in CO_2 emission reduction.[10] Furthermore, spinel ferrite is difficult to deoxidize, has paramagnetic and semiconducting character, which lead to its use both as an active component of a catalyst or as a carrier. In the face of increasingly serious environmental problems, many research groups have growing interest in the application of spinel ferrite in the technology of liquid phase catalysis in water treatment.[9] Although these teams have achieved some results, they have not made a breakthrough. One reason is that the size, morphology, composition, dispersion, surface features, and capabilities of the magnetic nanoparticles with spinel structure that they used cannot meet the needs of further practical applications. Therefore, the research on the ferrite nanoparticles to enable practical applications has an important and realistic significance. We obtained adsorption data in a raw solution, which is more accurate and is better suited for the practical application of removing organic pollutants and heavy metal ions from waste water. Further application of the as-prepared nanospheres in water treatment is likely.

In the face of increasingly serious environmental problems, considerable attention has been paid to pollution control by water treatment. Taking advantage of magnetic separation to clean waste water is a relatively new water treatment technology. The main indicators of water pollution are COD, and the presence of the five heavy metals (Hg^+, Cr^{6+}, Pb^{2+}, As^{5+}, and Cd^{2+}), ammonia, cyanide, volatile phenols, etc. Chemical oxygen demand (COD) is the main parameter to assess the organic content in waste water; The higher the COD value, the more serious the organic pollution in water. These organic pollutants are difficult to break down and toxic to aquatic and human life.[11,12] Traditional approaches for water treatment, such as biological degradation,[13,14] acidification,[15] electrochemical degradation,[16] chemical precipitation,[17] activated carbon adsorption,[18,19] ozone oxidation,[20,21] are generally restricted by high operating costs, low efficiency, or sensitivity to treatment conditions. By making use of the high separation efficiency characteristic of magnetic nanoparticles, the separation and detection of the toxic components of waste water can effectively reduce the workload and shorten the working hours.

[a] Key Laboratory of Automobile Materials (Jilin University), Ministry of Education and School of Materials Science and Engineering, Jilin University,
Changchun 130022, China
Fax: +86-431-85095876
E-mail: lijunzhao@jlu.edu.cn
[b] College of Chemistry, Jilin University,
Changchun 130023, P. R. China

The morphology of magnetic nanoparticles strongly influences their properties, because various crystal surfaces of nanoparticles can have very different atomic arrangements and electronic structures, leading to drastically different properties, and the requirements for most applications strongly depend on the shape, size, and magnetization of the magnetic nanoparticles. In this contribution, 50 nm $MnFe_2O_4$ nanospheres and 200 nm $MnFe_2O_4$ octahedra with saturation magnetizations of 79 emu/g and 58.7 emu/g, respectively, were separately prepared by the solvothermal method. To the best of our knowledge, 1 μm $MnFe_2O_4$ octahedra with a saturation magnetization of 68 emu/g were synthesized by a TEA-assisted hydrothermal route and reported by Zhang et al.;[22] 200 nm $MnFe_2O_4$ spheres with a saturation magnetization 60 emu/g were synthesized by Yadong Li et al. by using the solvothermal method. This is the first report on the solvothermal synthesis of regular $MnFe_2O_4$ spherical nanoparticles with such high saturation magnetizations. The adsorption characteristics of these nanospheres have been investigated in this paper. By further magnetic and adsorptive characterization, it can be expected that the $MnFe_2O_4$ ferrite nanocrystals could be used as catalysts or catalytic carriers in water treatment.

Results and Discussion

Characterization of $MnFe_2O_4$ Nanoparticles

Figure 1 shows a typical low-magnification SEM image of $MnFe_2O_4$ ferrite nanocrystals, from which we can conclude that octahedral structures are the exclusive products, which means that the $MnFe_2O_4$ nano-octahedra can be prepared on a large scale. The purity and crystallinity of the synthesized $MnFe_2O_4$ nanoparticles were examined by powder XRD, as shown in Figure 1b. All the diffraction peaks in the XRD pattern of the products can be indexed to the face-centered cubic structure of jacobsite ferrite (JCPDS No. 10-0319). The sharpness of the X-ray diffraction peaks confirms that the material should be highly crystallized $MnFe_2O_4$ without any other impurities.

Further insight into the morphology and microstructure of the $MnFe_2O_4$ nano-octahedra was gained by using TEM and HRTEM. Figure 1c shows the TEM image of $MnFe_2O_4$ nano-octahedra with edge lengths around 200 nm. HRTEM was performed on an individual $MnFe_2O_4$ particle, as shown in Figure 1d. The clear and run-through lattice fringes demonstrate that the nano-octahedron is essentially single crystalline with no crystal defects. The lattice spacing between two adjacent fringes is 0.234 nm, corresponding to the spacing of (222) planes of $MnFe_2O_4$. In principle, a crystal growth process consists of nucleation and growth, which are affected by the intrinsic crystal structure and the external conditions. It is well known that spinel $MnFe_2O_4$ is cubic in structure, the well-defined octahedral morphology is characteristic of cubic-structured crystals bound by eight (111) planes. Because of the slow reaction rate under the present solvothermal synthesis conditions and in the absence of other structure-modifying ions, octahedra with entirely {111} faces are considered to be the thermodynamically favorable product structures.

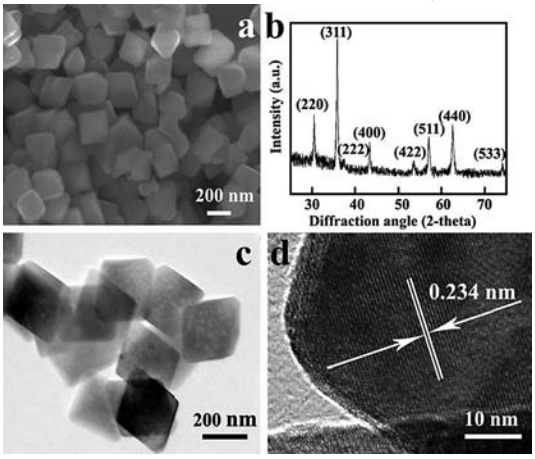

Figure 1. (a) SEM image, (b) XRD pattern, (c) TEM image, and (d) HRTEM image of $MnFe_2O_4$ ferrite nano-octahedra.

A possible reaction mechanism is proposed. $N_2H_4{\cdot}H_2O$ was successfully used for the syntheses of a variety of nanoscale metal materials, because it possesses strong reducing ability, a low concentration of impurities and has a low cost. $N_2H_4{\cdot}H_2O$ can serve as either an oxidant or a reducing agent in a synthetic route.[23]

As an oxidant: $N_2H_4 + 2H_2O + 2e^- = 2NH_3 + 2OH^-$ $\Phi° = 0.1$ V

As a reducing agent: $N_2 + 4H_2O + 4e^- = N_2H_4 + 4OH^-$ $\Phi° = -1.15$ V

$\Phi°$ is the criterion electromotance. $N_2H_4{\cdot}H_2O$, therefore, is able to show reducing ability in a highly alkaline medium. In the synthetic route, the molar ratio of Fe^{2+} to Mn^{7+} is 2:1; thus, in the precursor reaction of Fe^{2+} and Mn^{7+}, they first react as shown in Equations (1) and (2).

$$Mn^{7+} + 2Fe^{2+} \rightarrow Mn^{5+} + 2Fe^{3+} \quad (1)$$

$$Fe^{3+} + 3OH^- \rightarrow Fe(OH)_3 \rightarrow Fe(OH)_4^- \quad (2)$$

The presence of N_2H_4 causes Mn^{5+} to be reduced to Mn^{2+}. Then, Mn^{2+} and Fe^{3+} form $MnFe_2O_4$ [Equations (3) and (4)].

$$Mn^{2+} + OH^- \rightarrow Mn(OH)_2 \rightarrow Mn(OH)_3^- \quad (3)$$

$$Mn(OH)_3^- + 2Fe(OH)_4^- \rightarrow MnFe_2O_4 + 4H_2O + 3OH^- \quad (4)$$

To understand the formation mechanism of the octahedral $MnFe_2O_4$ nanoparticles, alkalinity-dependent experiments were carried out. The shape evolution of $MnFe_2O_4$ ferrite is shown in Figure 2. In this system, KOH was selected to alter the alkalinity. Control synthesis experiments were carried out by decreasing the amounts of KOH from 3.5 g (Figure 2a) to 1 g (Figure 2f) when other experimental parameters (solvent, temperature, reaction time, etc.) were fixed. It was found that alkalinity plays an important role in the formation of the nano-octahedral $MnFe_2O_4$ ferrite.

Compared with the SEM image in Figure 1, the images of the $MnFe_2O_4$ ferrite prepared with certain concentrations of KOH showed bad dispersity and irregular shapes. Herein, KOH behaves not only as a mineralizer but also as a surfactant in the solvothermal process. High concentrations of hydroxide easily adsorb onto (111) facets, which are then stabilized and grow slowly; hence, the growth of other facets will gradually diminish.[24] As a result, decreasing the amounts of KOH decreases the amount of hydroxide and weakens the selective adsorption on (111) facets. Accordingly, irregular shapes are formed. When the concentration of KOH drops below a certain value, the action of preferential adsorption on the (111) crystal planes will be weakened. The crystallites are prone to growth along dissimilar directions, so the spherical morphology may be more easy to achieve.

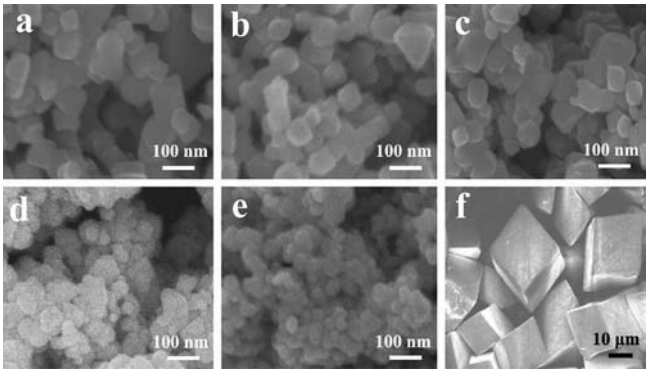

Figure 2. SEM images of $MnFe_2O_4$ ferrite obtained by using different amounts of KOH: (a) 3.5 g, (b) 3.0 g, (c) 2.5 g, (d) 2 g, (e) 1.5 g and (f) 1.0 g.

In fact, irregular spherical particles were obtained with the decrease in KOH concentration. However, to our surprise, when the amount of KOH was reduced to 1 g, it is interesting to note that the morphology of particles presented a fancy hexahedral shape (Figure 2f). The XRD patterns could be indexed to $KFeO_2$ (JCPDS 39-0892), Fe_2O_3 (JCPDS 21-0920), and Mn_3O_4 (JCPDS 24-0734). The alkalinity affects the balance between the chemical potential and the rate of ionic motion in the precursor solution, and a high concentration of KOH accelerates the nucleation.[25] We speculate that a certain concentration of hydroxide has a key role in forming the $MnFe_2O_4$ nucleus. With the decrease of hydroxide, $MnFe_2O_4$ can no longer be formed. In this case, $Fe(OH)_3$ and $Mn(OH)_2$ deposit first, then $Fe(OH)_3$ reacts with a small amount of residual hydroxide: $Fe(OH)_3 + KOH \rightarrow KFeO_2 + H_2O$. Superfluous $Fe(OH)_3$ precipitates as Fe_2O_3. $Mn(OH)_2$ cannot form the $MnFe_2O_4$ with $Fe(OH)_3$, so that some of the $Mn(OH)_2$ is oxidized by oxygen in the air to form the MnOOH, which then reacts as follows:

$$Mn(OH)_2 + 2MnOOH \rightarrow Mn_3O_4 + 2H_2O$$

Because the surface energy of the nanoparticles is generally high, the nanoparticles prefer to self-assemble with each other to form rugged microcrystals to reduce the high surface energy.[26] Then a hexahedron is formed by the rugged microcrystals.

In order to understand the shape control of the $MnFe_2O_4$ nanoparticles in the reaction system, further work is still in progress.

To contrast the effect of solvent, we also carried out a series of experiments with the solvent (EG) substituted by distilled water. It was found that both irregular micro-octahedra and nanospheres were prepared with 1.5 to 4.0 g of KOH. With the increase in KOH concentration, the amount of micro-octahedra increased, but that of nanospheres decreased. Down to 1.0 g KOH, regular and uniform $MnFe_2O_4$ nanospheres with around 50 nm diameter were fabricated. Figure 3a shows the SEM image of $MnFe_2O_4$ ferrite spherical nanoparticles. The size distribution range of the nanospheres is narrow. All the diffraction peaks in the XRD pattern (Figure 3b) of the products can be indexed to the face-centered cubic structure of jacobsite ferrite (JCPDS No. 10-0319). The average sizes of the $MnFe_2O_4$ nanospheres obtained from the calculation by the Scherer equation based on FWHM (full width at half-maximum) of the major diffraction peaks observed in Figure 3b is about 50 nm. This value is consistent with the results of the SEM and TEM analyses.

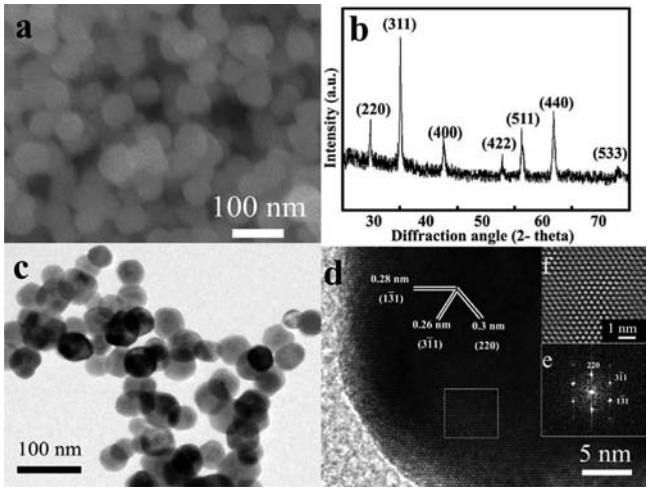

Figure 3. (a) SEM image, (b) XRD pattern, (c) TEM image, and (d) HRTEM image of $MnFe_2O_4$ nanospheres; (e) Fourier transform of the selected area framed in (d), and (f) reconstruction of the lattice by inverse Fourier transformation using only indexed diffraction spots in (e).

A typical TEM image of $MnFe_2O_4$ spherical nanoparticles can be observed in Figure 3c. The HRTEM images (Figure 3d) and the corresponding fast-Fourier-transform (FFT) patterns of a selected area of the image, which is indicated by a square frame in Figure 3d, is shown in the inset in Figure 3e; it represents a pattern of diffraction spots with hexagonal symmetry. Figure 3f shows the reconstruction of the lattice within the selected area by inverse Fourier transform using only the indexed diffraction spots in Figure 3e. The clear lattice fringes can prove the high crystallinity of the as-prepared nanospheres. The dominant exposed planes of $MnFe_2O_4$ spheres are {114}. The lattice

spacing between two adjacent fringes that can be observed corresponds to the set of (220) planes with a lattice spacing of 0.3 nm, the set of (311) planes with a lattice spacing of 0.27 nm, and the set of (222) planes with 0.24 nm spacing, which can be determined as the [110], [311], and [131] crystallographic directions, respectively. The crystal grows along the three directions evenly. Both HRTEM images and diffraction patterns confirm that the $MnFe_2O_4$ nanospheres are single-crystalline.

It is known that the physical and chemical properties of the solvent can influence the solubility, reactivity, and diffusion behavior of the reagents, and even the growth morphologies of product.[27] Spinel ferrites all have face-centered cubic structure, and thus no crystallographic driving force for anisotropic growth; therefore, they should assemble to form faceted spheres rather than octahedra.[14] Compared with the EG solvent in which we obtained the hexahedral nanoparticles (Figure 1), the water dissociation has made up for the deficiency in hydroxy groups. All the hydroxy groups are involved in the formation of the sediment of $MnFe_2O_4$, so their ability of selective adsorption almost disappears. Instead, the nucleus grows along the crystal axis evenly, thus forms the nanospheres.

Magnetic Properties of $MnFe_2O_4$ Nanoparticles

Magnetic properties of the as-synthesized $MnFe_2O_4$ nano-octahedra and nanospheres were measured at room temperature, and both samples showed a typical hysteresis loop in their magnetic behavior, as observed in Figure 4. The insets are magnified views of the hysteresis loops at low applied fields. Both nanoparticles show ferromagnetic behavior. This hysteresis loop is typical of soft magnetic materials; the very small area surrounded by the closed curve is related to the soft magnetic properties of materials. The saturation magnetization (M_s), remanent magnetization (M_r), and coercivity (H_c) values of $MnFe_2O_4$ nano-octahedra (Figure 4a) and nanospheres (Figure 4b) are 58.7 emu/g, 7.1 emu/g, 86 Oe, and 79 emu/g, 6 emu/g, 77 Oe, respectively. The H_c values for two samples are less than the value for bulk ferrite,[28] which is in accord with the properties of soft magnetic materials. The difference in M_s values may be attributed to the interior microstructure. At the same time, our experiments confirm that the morphology is one of the main factors that determine the magnetic properties of the magnetite. The saturation magnetization of $MnFe_2O_4$ spherical structures is 79 emu/g, which is among the best values reported so far. Because of the small size and the high saturation magnetization of the spherical particles, we expect that they could have important applications in water treatment.

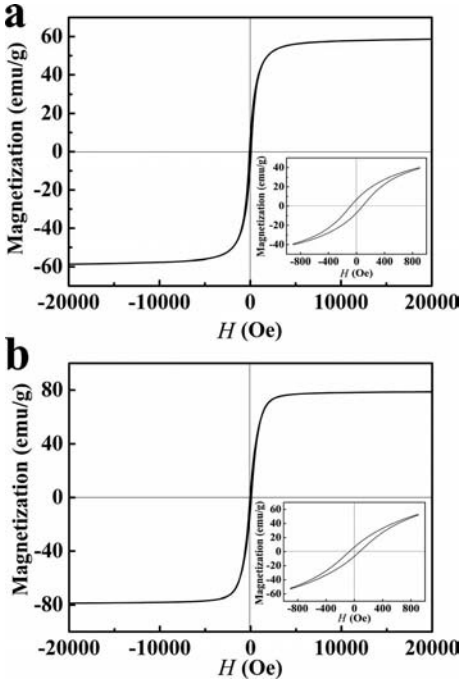

Figure 4. Room-temperature hysteresis loops of (a) as-prepared $MnFe_2O_4$ octahedra and (b) spheres. The insets are magnified views of the hysteresis loops at low applied fields.

Adsorption Properties of $MnFe_2O_4$ Nanoparticles

In the first place, we chose Congo red as a typical organic pollutant. A calibration curve was used to evaluate the adsorption values during the reaction. To ensure the accuracy, reliability, and reproducibility of the collected data, the adsorption experiments were carried out at least three times, and the average values of the three data sets are presented. In a typical experiment, Congo red solutions with different concentrations were prepared first. UV/Vis absorption spectra (Shimadzu UV-1601PC) were used to record the absorbency of the above solutions and to construct a calibration equation. When the concentration of Congo red was less than 30 mg/L, the concentration versus absorbency plot was linear; therefore, 30 mg/L was chosen as the initial concentration. The curve in Figure 5a shows that when 20 mg of as-obtained nanosphere was added to 40 mL of Congo red solution with an initial concentration of 30 mg/L at room temperature (20 °C), over 87% of Congo red can be removed within 60 min. The adsorption capacity was measured as 39.3 mg Congo red per gram of nanospheres. It can be found from Figure 5a that the most of the Congo red has been adsorbed after 5 min. This fast removal rate is mainly attributed to the electrostatic attraction between the surface of the particles and the Congo red species in solution[29] and the high surface area available as a result of the small particle size. Furthermore, $MnFe_2O_4$ nanoparticles can easily be removed from the reaction media by applying an external magnetic field. As shown in the inset in Figure 5a, when a magnet was placed close to the reaction vessel for a while, it could be observed that the samples synthesized were rapidly attracted, and a nearly colorless solution remained. This demonstrates the efficacy of the magnetic separation, which could be used in water treatment.

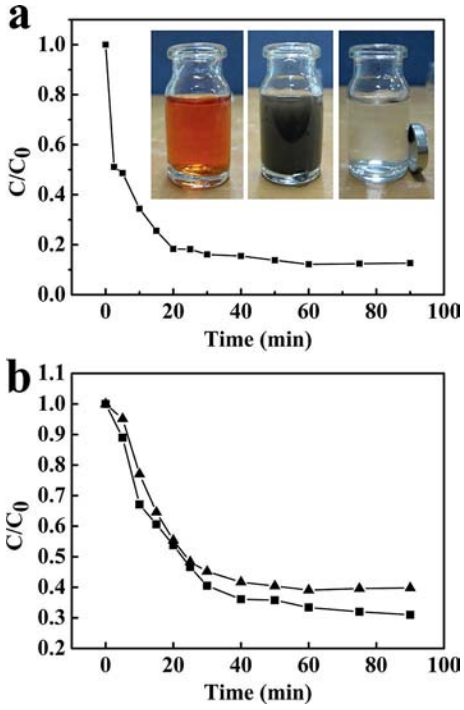

Figure 5. (a) Adsorption rate of Congo red on as-prepared manganese ferrite nanoparticles. The inset shows photos of the Congo red solution at different times, from left to right: 0 min, immediately after mixing with the magnetic nanoparticles, 90 min. (b) Adsorption rate of Cr^{VI} (triangles) and Pb^{II} (squares) on the as-prepared $MnFe_2O_4$ nanospheres.

Removal of highly toxic pollutants from water is also of great importance. Chromium and lead were chosen as representative pollutant ions. Atomic absorption spectroscopy was used to determine the concentrations of these pollutant ions, and a calibration curve was prepared. Under similar experimental conditions, the nanospheres (40 mg) were added to Cr^{VI} or Pb^{II} solution (50 mL, 10 mg/L) whilst stirring. Adsorption curves are shown in Figure 5b. The adsorption capacity of the as-prepared spherical particles in 60 min was 7.6 mg/g for Cr^{VI} and 8.3 mg/g for Pb^{II}. In the preparation process, the existence of hydroxide causes a large number of negative charges on the surface of the as-prepared nanoparticles. The electrostatic attraction between the metal cation and the particles ensure the adsorption. It is worth mentioning that many studies test the adsorption with pH lower than 4 to improve the adsorption capacity of the sorbent.[30] In contrast, in our experiments, raw solutions were used, the data obtained was more accurate and could better approximate the conditions in the practical application.

Conclusions

Uniform $MnFe_2O_4$ octahedral and spherical nanocrystals were prepared by a simple solvothermal process without the assistance of a surfactant. Both the concentration of hydroxide ions and the type of solvent play key roles in the formation of the nanostructure. A sufficient amount of NaOH and the presence of EG were necessary for the formation of the octahedral structures. With a low concentration of NaOH and H_2O as solvent, spheres could be obtained. In addition, both of the as-prepared products show ferromagnetic properties at room temperature. The as-prepared nanosphere has a good adsorption capacity for organic pollutants and heavy metal cations, which would make its use in the practical application of water treatment feasible.

Experimental Section

All chemicals were of analytical grade and were used without further purification. The chemicals were obtained from Beijing Chemicals Co. (Beijing, China). We used ferrous sulfate as the starting material, which was pro rata oxidized to ferric salts with $KMnO_4$, then alkalinized with NaOH. Hydrazine hydrate was used as reducing agent for the synthesis of $MnFe_2O_4$ ferrite nanocrystals. For the adsorption experiment, we used Congo red as a typical organic contaminant. $K_2Cr_2O_7$ and $PbSO_4$ were used as the sources of Cr^{VI} and Pb^{II}, respectively.

In a typical synthesis, iron sulfate heptahydrate ($FeSO_4 \cdot 7H_2O$) and potassium permanganate ($KMnO_4$) were mixed and dissolved in ethylene glycol (20 mL) to form a transparent solution, the molar ratio of Fe^{2+} and Mn^{7+} was 2:1, which is accurately equal to the theoretic molar ratio in the manganese ferrite magnetite molecule. During magnetic stirring, potassium hydroxide (KOH) was added to the above solution and reacted for 15 min, then hydrazine hydrate ($N_2H_4 \cdot H_2O$, 2 mL) was added into the resulting solution under vigorous stirring. After another 15 min of continuous stirring, the mixture was transferred into an autoclave, sealed, put into an oven, and kept at 260 °C for 24 h. After cooling to room temperature naturally, the black ferrite nanoparticles were separated by a magnet and washed twice with deionized water and ethanol.

The synthesized samples were subsequently characterized by X-ray diffraction (XRD, Rigaku D/max 2500pc X-ray diffractometer with Cu-K_α radiation, λ = 1.5406 Å), scanning electron microscopy (SEM, Hitachi S-4700), transmission electron microscopy (TEM, Philips Tecnai 20, 200 kV), and high-resolution transmission electron microscopy (HRTEM, JEOL-3010, 300 kV). Hysteresis loops were collected with a Quantum Design superconducting quantum interference device (SQUID) magnetometer (Lake Shore 7307) at 300 K. The SQUID measurements for all the samples were done on the pure and dried powders.

Nanospheres (20 mg) were added to Congo red solution (40 mL, 30 mg/L) whilst stirring, and UV/Vis absorption spectra (Shimadzu UV-1601PC) were recorded at different intervals to monitor the process. For the adsorption of the salts of heavy metals, Cr^{VI} and Pb^{II} solutions with initial concentrations of 10 mg/L were prepared. Then, the adsorbent sample (40 mg) was added to the above solutions (50 mL) whilst stirring. After a specified time, the solid and liquid were separated, and the chromium and lead concentrations in the remaining solutions were measured with a TAS-986 atomic absorption spectroscope.

Acknowledgments

We acknowledge support by the Natural Science Foundation of Jilin Province.

[1] M. Sugimoto, *J. Am. Ceram. Soc.* **1999**, *82*, 269.
[2] M. P. Pileni, *Adv. Funct. Mater.* **2001**, *11*, 323.
[3] M. D. Shultz, S. Calvin, P. P. Fatouros, S. A. Morrison, E. E. Carpenter, *J. Magn. Magn. Mater.* **2007**, *311*, 464.
[4] D. L. Zhao, Q. Lv, Z. M. Shen, *J. Alloys Compd.* **2009**, *480*, 634–638.
[5] C. Liu, B. S. Zou, A. J. Rondinone, Z. J. Zhang, *J. Phys. Chem. B* **2000**, *104*, 1141.
[6] L. S. Zhong, J. S. Hu, H. P. Liang, A. M. Cao, W. G. Song, L. J. Wan, *Adv. Mater.* **2006**, *18*, 2426–2431.
[7] S. S. Lv, X. G. Chen, Y. Ye, S. H. Yin, J. P. Cheng, M. S. Xia, *J. Hazard. Mater.* **2009**, *171*, 634–639.
[8] K. Faungnawakij, Y. Tanaka, N. Shimoda, T. Fukunaga, R. Kikuchi, K. Eguchi, *Appl. Catal. B* **2007**, *74*, 144–151.
[9] T. Valdés-Solís, P. Valle-Vigón, S. Álvarez, G. Marbán, A. B. Fuertes, *Catal. Commun.* **2007**, *8*, 2037–2042.
[10] O. A. Fouad, K. S. Halim, M. M. Rashad, *Top. Catal.* **2008**, *47*, 61–65.
[11] G. Jungclaus, V. Avila, R. Hites, *Environ. Sci. Technol.* **1978**, *12*, 88–96.
[12] M. Pera-Titus, V. Garcia-Molina, M. A. Banos, J. Gimenez, S. Esplugas, *Appl. Catal. B* **2004**, *47*, 219–256.
[13] M. Bajaj, C. Gallert, J. Winter, *Bioresour. Technol.* **2008**, *99*, 8376–8381.
[14] T. M. Lapara, J. E. Alleman, *Water Res.* **1999**, *33*, 895–908.
[15] H. Q. Yu, H. P. Fang, *Appl. Microbiol. Biotechnol.* **2000**, *54*, 439–444.
[16] G. H. Chen, *Sep. Purif. Technol.* **2004**, *38*, 11–41.
[17] Z. Q. Jia, Y. Li, S. Lu, H. Z. Peng, J. Y. Ge, S. D. Chen, *J. Hazard. Mater.* **2006**, *129*, 234–238.
[18] R. R. Bansode, J. N. Losso, W. E. Marshall, R. M. Rao, R. J. Portier, *Bioresour. Technol.* **2004**, *94*, 129–135.
[19] X. Wang, N. Zhu, B. Yin, *J. Hazard. Mater.* **2008**, *153*, 22–27.
[20] J. L. Gong, Y. Liu, X. B. Sun, *Water Res.* **2008**, *42*, 1238–1244.
[21] S. Meric, D. Kaptan, T. Olmez, *Chemosphere* **2004**, *54*, 435–441.
[22] D. E. Zhang, X. J. Zhang, X. M. Ni, J. M. Song, H. G. Zheng, *Chem. Phys. Lett.* **2006**, *426*, 120–123.
[23] K. Takiyama, *Bull. Chem. Soc. Jpn.* **1958**, *31*, 950.
[24] L. J. Zhao, H. J. Zhang, J. K. Tang, S. Y. Song, F. Cao, *Mater. Lett.* **2009**, *63*, 307–309.
[25] X. Y. Hou, J. Feng, X. D. Xu, M. L. Zhang, *J. Alloys Compd.* **2010**, *491*, 258–263.
[26] Y. Zhu, W. Zhao, H. Chen, J. Shi, *J. Phys. Chem. C* **2007**, *111*, 5281.
[27] Z. P. Liu, J. B. Liang, S. Li, S. Peng, Y. T. Qian, *Chem. Eur. J.* **2004**, *10*, 634.
[28] T. Sato, S. Ishibashi, *Int. J. Miner. Process.* **2001**, *62*, 95.
[29] F. Herrera, A. Lopez, G. Mascolo, E. Albers, J. Kiwi, *Appl. Catal. B* **2001**, *29*, 147.
[30] L. S. Zhong, J. S. Hu, H. P. Liang, A. M. Cao, W. G. Song, L. J. Wan, *Adv. Mater.* **2006**, *18*, 2426–2431.

Received: March 1, 2011
Published Online: May 18, 2011

